Geometric Mechanics of Origami Patterns Exhibiting Poisson's Ratio Switch by Breaking Mountain and Valley Assignment

Phanisri P. Pratapa, Ke Liu, and Glaucio H. Paulino

Phys. Rev. Lett. **122**, 155501 — Published 19 April 2019

DOI: 10.1103/PhysRevLett.122.155501

Geometric mechanics of origami patterns exhibiting Poisson's ratio switch by breaking Mountain/Valley assignment

Phanisri P. Pratapa,* Ke Liu,* and Glaucio H. Paulino†
School of Civil and Environmental Engineering, Georgia Institute of Technology, Atlanta, GA 30332, USA
(Dated: February 4, 2019)

Exploring the configurational space of specific origami patterns (e.g. Miura-Ori, Eggbox) has led to major advances in science and technology. To augment the origami design space, we present a pattern, named *Morph*, that combines the features of its parent patterns. We introduce a four-vertex origami cell that morphs continuously between a Miura mode and an Eggbox mode, forming a homotopy class of configurations. This is achieved by changing Mountain/Valley assignment of one of the creases, leading to a smooth switch through a wide range of negative and positive Poisson's ratios. We present elegant analytical expressions of Poisson's ratios for both in-plane stretching and out-of-plane bending, and find that they are equal in magnitude and opposite in sign. Further, we show that by combining compatible unit cells in each of the aforementioned modes through kinematic bifurcation, we can create hybrid origami patterns that display unique properties such as topological mode-locking (irreversible morphing under stretch by synchronized engagement of aligned panels in the Miura mode) and tunable switching of Poisson's ratio.

Origami-inspired geometries have been used to design metamaterials with unusual properties [1–7]. The aesthetically pleasant patterns and shapes typically start from 2D sheets to construct 3D structures according to mountain and valley assignments encoded in the crease patterns. In this letter, we present a new periodic pattern, named *Morph*, with a non-developable degree-4 unit cell that allows a certain crease to switch its mountain/valley assignment, leading to properties such as arbitrarily tunable Poisson's ratio that spans from positive to negative, and topological mode-locking.

Owing to their special geometries, origami metamaterials usually display interesting behavior [8–11]. For instance, the Miura-ori exhibits a negative Poisson's ratio under in-plane deformations [9], while the standard Eggbox pattern has a positive Poisson's ratio [12, 13]. In comparison, our proposed pattern morphs continuously between a Miura mode and an Eggbox mode (see Fig. 1), thus behaving as a single material possessing both positive and negative Poisson's ratio. The Poisson's ratio switching is an enticing phenomenon that has only been found recently for selected mechanical metamaterial designs, including nanoplates [14], re-entrant origami tube assemblages [15], bistable auxetics [16], kirigami structures [17] and soft networks [18]. Compared to other designs, the Morph excels on having a wider tunable range of Poisson's ratio, theoretically from negative infinity to positive infinity. In addition, the Morph unit cells can be assembled to form 2D tessellations in which the unit cell can stay either in the Miura or Eggbox mode, which allows the formation of hybrid patterns – achieved by harnessing kinematic bifurcation.

In their most general form, the panel angles α and β of the Morph pattern are two independent geometric parameters (see Fig. 1), thereby enriching the origami design space; unlike the standard cases such as Eggbox ($\beta = \alpha$) or Miura-ori ($\beta = \pi - \alpha$) whose vertex geometry is dictated by just a single parameter α.

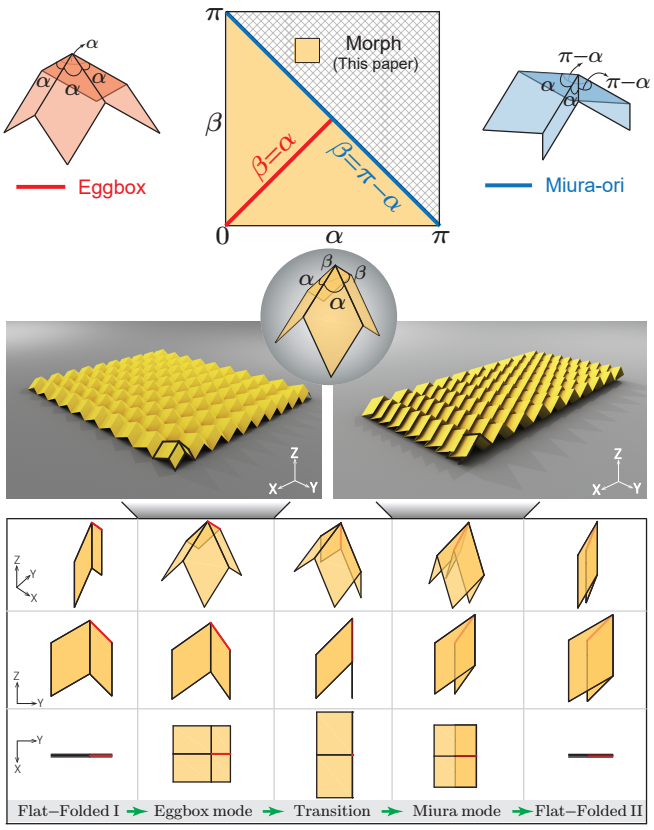

FIG. 1. (Top) Expanded design space of the Morph pattern (yellow shading) with standard Eggbox (red line) and Miura-ori (blue line) as particular cases. (Middle) Fundamental modes of the Morph pattern: Eggbox mode (left) and Miura mode (right). (Bottom) Configuration space showing transition of the Morph unit cell from one flat-folded state to another (see supplementary Movie 1). The crease line shown in red morphs from a mountain fold in the Eggbox mode to a valley fold in the Miura mode.

Additionally, for $\alpha \neq \beta$, the degree-4 non-developability feature that the Morph shares with the standard Eggbox makes it a generalization of the basic pattern. Theoretically, the Poisson's ratio of the Morph sweeps the whole spectrum of real numbers as it morphs from one flat-folded state to the Eggbox mode, to the Miura mode, and to another flat-folded state, as shown in Fig. 1. The red crease in Fig. 1 changes its mountain/valley assignment as it *transitions* from Eggbox mode to the Miura mode, which is made possible owing to the fact that the angle β is smaller than the angle α of the other two panels. By contrast, the standard Eggbox or Miura-ori patterns do not allow any crease to switch its mountain/valley assignment.

To parametrize the rigid origami behavior of the Morph unit cell, we define angles ϕ, ψ as the angles between opposing crease lines and denote the dihedral angles between the panels as γ_1, γ_2, γ_3, γ_4, as shown in Fig. 2(a). The unit cell has a degree-4 vertex, and thus it is a single degree of freedom system. The dihedral angles are related to one another and to ϕ, ψ. We derive that $\gamma_2 = \gamma_4$, as $0 \leq \gamma_2, \gamma_4 \leq \pi$, indicating the existence of a plane of symmetry passing through the vertices denoted by O_4, O_5 and O_6. While $0 \leq \gamma_1 < \pi$, the ability of the crease O_5O_6 to switch between mountain and valley allows γ_3 to vary from 0 to 2π. In the flat-folded state I, $\phi = \phi_{max} = \alpha + \beta$ and $\gamma_3 = 0$. For $0 < \gamma_3 < \pi$, the unit cell is in Eggbox mode and O_5O_6 is a mountain crease. As γ_3 passes through π, O_5O_6 transitions from a mountain to a valley crease and the panels on either side of O_5O_6 become coplanar. In the transition state, angle ψ also reaches its maximum $\psi_{max} = 2\beta$. For $\pi < \gamma_3 < 2\pi$, the unit cell is in Miura mode and O_5O_6 is a valley crease. Finally, as $\gamma_3 \to 2\pi$, the unit cell approaches the flat-folded II state with $\phi = \phi_{min} = \alpha - \beta$. Let us define two intermediate variables:

$$\xi = \cos\beta - \cos\alpha\cos\phi = \sin\alpha\sin\phi\cos(\gamma_1/2), \quad (1)$$

$$\zeta = \cos\alpha - \cos\beta\cos\phi = \sin\beta\sin\phi\cos(\gamma_3/2). \quad (2)$$

The configurational space of the Morph unit cell is then fully described by ϕ $(0 \leq \psi \leq 2\beta < \pi)$ and ψ $(0 < \alpha - \beta \leq \phi \leq \alpha + \beta < \pi)$ through the following equation:

$$\cos\psi = \cos 2\alpha + 2\xi^2 \csc^2\phi, \quad (3)$$

which is presented for various choices of panel angles in Fig. 2(b). We can observe in Fig. 2(b) that as $\alpha \to \beta$, the Miura mode vanishes.

We define the Poisson's ratio for in-plane stretching as the tangential ratio of the orthogonal strains measured by the change of width W and length L of a unit cell [8, 9], which are given by:

$$W = 2c\sin(\psi/2), \quad L = \sqrt{a^2 + b^2 - 2ab\cos\phi}. \quad (4)$$

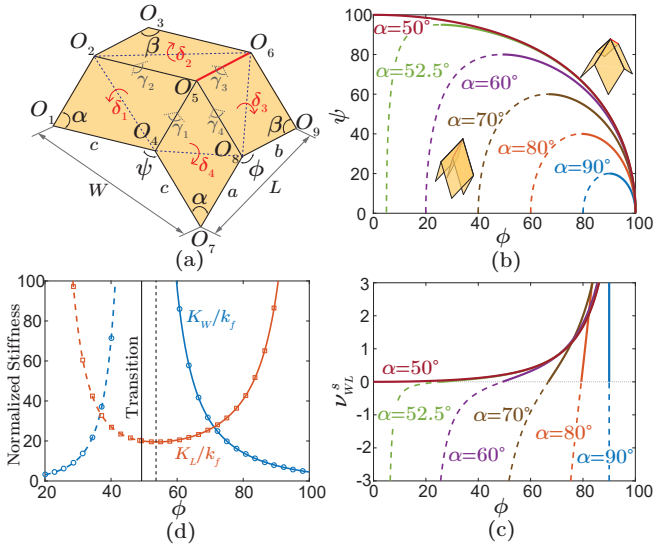

FIG. 2. Geometric configuration and in-plane mechanics of the Morph pattern. (a) Schematic of the unit cell with the description of geometric parameters and vertices. (b) & (c) represent the configuration space and Poisson's ratio in stretch, respectively, for different choices of α considering $\alpha + \beta = 100°$. The solid and dashed lines represent the Eggbox and Miura modes, respectively. (d) Stretching stiffness in **W** and **L** directions for $\alpha = 60°$, $\beta = 40°$. The markers represent numerical results from origami structural analyses using the bar-and-hinge reduced order model [19]. We assume that $a = c = 1$.

To assure the bounding box of a unit cell being orthorhombic, which requires for example, $O_1O_4O_7 \perp O_1O_7O_9O_3$ and $O_1O_2O_3 \perp O_1O_7O_9O_3$, the panel dimensions a and b are constrained by $b = a|\cos\alpha/\cos\beta|$ (see Section I of the Supplementary Material). The analytical expression for the in-plane Poisson's ratio when stretching in the **L** direction is

$$\nu^s_{WL} = -\frac{\mathrm{d}W/W}{\mathrm{d}L/L} = \frac{4c^2L^2}{a^2W^2}\left|\frac{\cos\beta}{\cos\alpha}\right|\frac{\xi\zeta}{\sin^4\phi}. \quad (5)$$

As plotted in Fig. 2(c), it is clear that the stretching Poisson's ratio is negative in the Miura mode and positive in the Eggbox mode, with a smooth transition near 0. Theoretically ν^s_{WL} approaches $-\infty$ or $+\infty$ in the two flat-folded limits, thereby leading to a wide range of tunability. We note that, since W^2/c^2 and L^2/a^2 do not depend on the length dimensions of the unit cell, the Poisson's ratio of the unit cell depends only on α, β and ϕ making it a purely geometric quantity that is also independent of length scale of the pattern.

Accordingly, assuming that the energy of the unit cells is comprised of deformation from linear elastic rotational hinges along the crease lines, we can derive the linear in-plane stretching stiffness of the pattern. Denoting k_f as the rotational spring modulus, the stored energy of the

system is given by

$$\mathcal{U}_s = \frac{k_f}{2}\left[a(\gamma_1-\gamma_{1,0})^2 + b(\gamma_3-\gamma_{3,0})^2 + 2c(\gamma_2-\gamma_{2,0})^2\right], \tag{6}$$

where $\gamma_{1,0}$, $\gamma_{2,0}$, and $\gamma_{3,0}$ are the natural dihedral angles in the undeformed state. Expressing γ_2 and γ_3 in terms of γ_1, the stiffnesses along **L** direction is derived as:

$$K_L = \left.\frac{\mathrm{d}^2\mathcal{U}_s}{\mathrm{d}L^2}\right|_{L=L_0} = \left.\frac{\mathrm{d}^2\mathcal{U}_s}{\mathrm{d}\gamma_1^2}\left(\frac{\mathrm{d}L}{\mathrm{d}\phi}\frac{\mathrm{d}\phi}{\mathrm{d}\gamma_1}\right)^{-2}\right|_{\gamma_1=\gamma_{1,0}}. \tag{7}$$

Similarly, we can get the stiffness along the **W** direction (see Section II of the Supplementary Material). As shown in Fig. 2(d), the in-plane stiffness in the **W** direction (denoted by K_W) is minimum at flat-folded states and reaches maximum at the transition state. Interestingly, while K_L is maximal at flat-folded states, it is only close to minimum at the transition but slightly away towards the Eggbox mode.

As revealed in previous research [8, 9, 12], kinematically single Degree of Freedom (DOF) origami pattern may experience out-of-plane deformation, other than pure (in-plane) folding, if compliance of panels is taken into consideration. Accordingly, we define the Poisson's ratio in bending as the ratio of principal curvatures ($\nu^b_{WL} = -\kappa_W/\kappa_L$) and find that the Morph pattern features a saddle shaped geometry in the Miura mode, and a dome shape geometry in the Eggbox mode (see Figs. 3(a),(b)). It is intriguing that the Morph pattern exhibits distinct Poisson's ratio in stretching and bending, similar to what have been found, separately, with the standard Miura-ori and the standard Eggbox patterns. Here we show that, just like its two extreme cases [9, 12], the Morph pattern displays Poisson's ratio with opposite sign but equal magnitude in stretching and bending. We can analytically calculate the principal bending curvatures by allowing each panel of the origami pattern to bend along one of its diagonals [9], under the assumption of infinitesimal deformation.

We add infinitesimal rotations δ_1, δ_2, δ_3, δ_4 as shown in Fig. 2(a) to provide further DOFs to the system in order to simulate bending of panels. Hence, there are in total 4 extra DOFs being added, yet isometric deformation is still ensured. Bending of the unit cell shall preserve the orthogonality between the two sides of a unit cell (i.e. **L** and **W**). Thus we enforce that the normals of the side triangles of a unit cell after bending (e.g. $\Delta O_1'O_2'O_3'$, $\Delta O_7'O_8'O_9'$, $\Delta O_1'O_4'O_7'$, $\Delta O_3'O_6'O_9'$) remain orthogonal to their respective side directions, which leads to three independent constraints:

$$a\xi\frac{\delta_1}{\ell_1} = b\zeta\frac{\delta_2}{\ell_2},\ b\zeta\frac{\delta_3}{\ell_3} = a\xi\frac{\delta_4}{\ell_4},\ \frac{\delta_1}{\ell_1} = \frac{\delta_4}{\ell_4}, \tag{8}$$

where, ℓ_1, ℓ_2, ℓ_3, ℓ_4 are the lengths of the diagonals O_2O_4, O_2O_6, O_6O_8 and O_4O_8, respectively. Thus, the bending is uniquely defined up to a single DOF. These constraints automatically ensure that the deformed unit cell can be periodically tessellated in the two principal directions (i.e. **L** and **W**), that is, $\angle O_1'O_2'O_3' = \angle O_7'O_8'O_9'$ and $\angle O_1'O_4'O_7' = \angle O_3'O_6'O_9'$.

The curvatures in **L** and **W** directions are determined by:

$$\kappa_L = -\frac{|\theta_{147}| \pm |\theta_{369}|}{L}, \tag{9}$$

$$\kappa_W = -\frac{|\theta_{789}| + |\theta_{123}|}{W}, \tag{10}$$

where, the $'+'$ or $'-'$ in Eqn. 9 for κ_L depends on whether the system is in the Eggbox mode or the Miura mode respectively and θ_{147}, θ_{369}, θ_{789}, θ_{123} are the tilt angles (see Figs. 3(c),(d)). The bending Poisson's ratio is then obtained as (see Sections III and IV of the Supplementary Material):

$$\nu^b_{WL} = -\frac{\kappa_W}{\kappa_L} = -\frac{4c^2L^2}{a^2W^2}\left|\frac{\cos\beta}{\cos\alpha}\right|\frac{\xi\zeta}{\sin^4\phi}. \tag{11}$$

Comparing Eqn. 5 with Eqn. 11, we obtain the elegant result, $\nu^b_{WL} = -\nu^s_{WL}$ for the Morph pattern. The above expression reduces to standard Miura-ori [8, 9] and Eggbox [12] as two particular cases for appropriate choices of panel angles α and β (see Sections V and VI of the Supplementary Material).

The aforementioned bending mode allows us to analytically derive the bending stiffness of the Morph pattern, which has similar characteristics to the in-plane stretching stiffness (see Fig. S8 of the Supplementary Material). By performing numerical simulation using the reduced

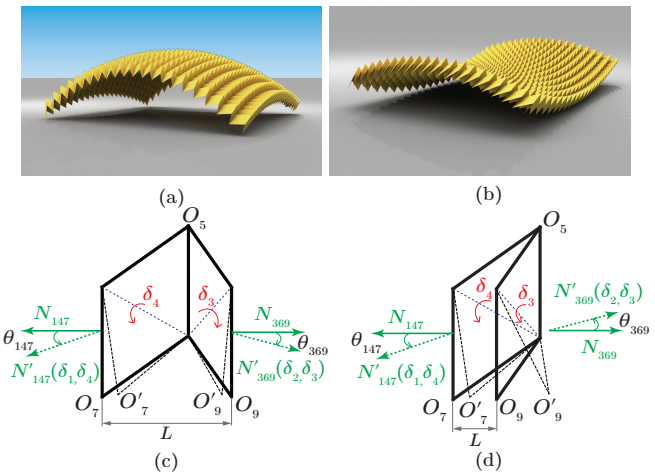

FIG. 3. Out-of-plane bending of the Morph pattern. (a) & (b) Bent shapes of the pattern in Eggbox and Miura modes respectively obtained using the bar-and-hinge origami model. (c) & (d) Triangular face tilts creating a net angle change across length L of the Morph pattern in Eggbox and Miura modes, respectively. The new coordinates of vertices O7 and O9 after bending (i.e. O_7' and O_9', respectively), can be calculated using the Rodrigues' rotation formula [20].

order bar-and-hinge model [19], we find that the analytical model agrees well with the numerical simulations with very small discrepancies, which further strengthens the assumption that infinitesimal rotations about panel diagonals are sufficient to characterize first order bending response of the Morph pattern.

Owing to its mode switching feature, the Morph pattern unit cells do not have to be tessellated with uniform configuration. It is kinematically admissible to couple the Morph unit cells into a *hybrid pattern*, such that there are both Miura mode cells and Eggbox mode cells in a single tessellation, as demonstrated in Figs. 4(a),(b). The feasibility of such a system can be understood by noting that in Fig. 2(b), a given ψ, can correspond to the angle ϕ in either the Eggbox mode or the Miura mode which we denote as ϕ_e or ϕ_m respectively. These angles are given by $\phi_e = \phi_1 + \phi_2$ and $\phi_m = \phi_1 - \phi_2$, where ϕ_1, ϕ_2 are as shown in Fig. 4(c) and are given by $\cos\phi_1 = \cos\alpha/\cos(\psi/2)$, $\cos\phi_2 = \cos\beta/\cos(\psi/2)$ (see Section VII of the Supplementary Material).

In Fig. 4(c) we show that one can smoothly deform a homogeneous Morph pattern to a hybrid pattern using rigid origami motion (no panel bending). By compatibility, all the unit cells have the same ψ, i.e. $\psi_m = \psi_e = \psi$. Also, when $\phi_m = \phi_e$, all the unit cells of the pattern are either in the Miura mode or the Eggbox mode, depending on whether $\phi = \phi_m = \phi_1 - \phi_2$ or $\phi = \phi_e = \phi_1 + \phi_2$ respectively. In the figure, these configurations are represented by the straight line in blue and red colors respectively. As we move up the blue line, the ϕ_m increases and reaches the transition point (which is $\phi_T = \cos^{-1}(\cos\alpha/\cos\beta)$) between Miura and Eggbox modes. At this point, we note that there is kinematic bifurcation in the configuration space, which could either move all the unit cells into the Eggbox mode by uniformly increasing the angle ϕ further across all cells or switch some of the strips back into Miura mode and therefore generate hybrid patterns represented by the green curve in the figure. This process is also demonstrated through animations and partly through physical testing in Movies 2 and 4 respectively of the Supplementary Material. It can be seen that along the green curve, ϕ_m reduces and ϕ_e increases as to be expected from Fig. 2(b), for a compatible ψ, across the two types of unit cells in the system.

Depending on the coupling mode of the hybrid pattern, the tessellated sheet exhibits a different Poisson's ratio, $\nu^s_{WL,h}$ (see Eqn. S98 of the Supplementary Material). There exists a transition point when $\nu^s_{WL,h}$ varies from positive extremum (all unit cells in Eggbox mode) to negative extremum (all unit cells in Miura mode), which however, does not happen when the number of Miura mode and Eggbox mode strips are the same, due to unequal contributions from both the modes. We consider a system with 100×100 cells and increase the number of Miura mode cells (in strips) along the **L** direction (denoted as n_m) from 0 to 100 (see Fig. 4(d)). For a given

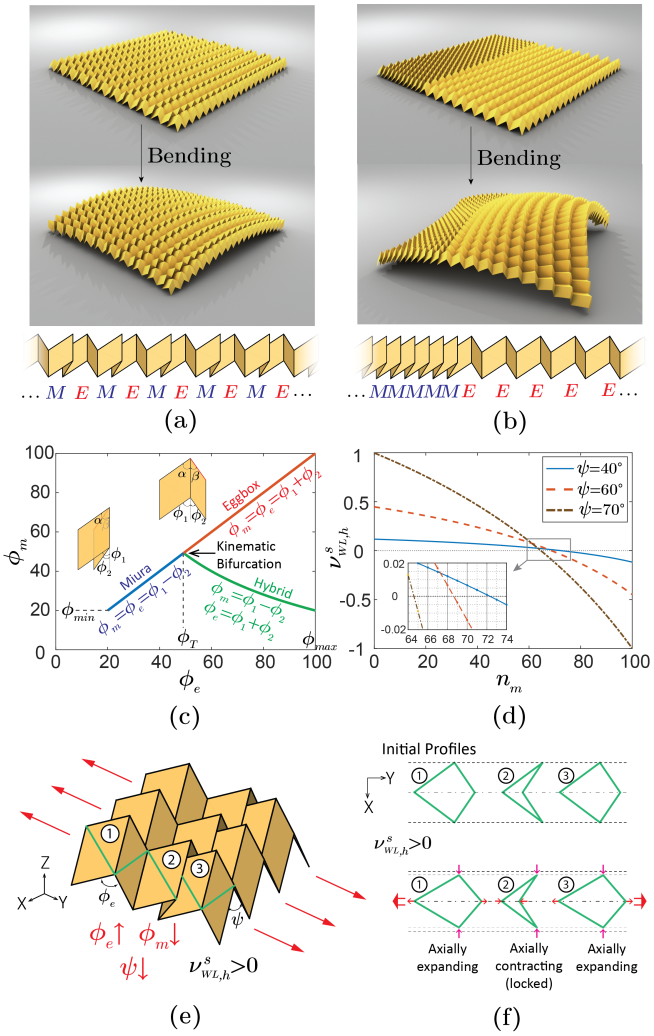

FIG. 4. Hybrid origami assemblages associated with the Morph pattern. (a) Alternating strips of Miura (M) and Eggbox (E) modes. (b) Half pattern with strips in Miura (M) mode and the other half in Eggbox (E) mode. (c) Creation of hybrid patterns from the Morph through kinematic bifurcation. (d) Change of Poisson's ratio with respect to varying number of Miura mode strips (n_m) in a hybrid mode with 100×100 unit cells. The notation $\nu^s_{WL,h}$ denotes the Poisson's ratio under stretch for the hybrid pattern. In (c), (d) we assume, $\alpha = 60°$, $\beta = 40°$. (e) & (f) Mode-locking due to extension in **L** direction when $\nu^s_{WL,h} > 0$. The positive global Poisson's ratio implies contraction in the **W** direction, resulting in decrease of ψ_e and ψ_m. The oppositely signed unit cell Poisson's ratios of the two modes indicates that while ϕ_e increases, ϕ_m decreases, meaning the Miura mode cells are axially contracting, opposite to the global axial deformation. The Miura mode cells with decreasing ϕ_m are locked because such cells can no longer smoothly transition to their Eggbox mode in a rigid origami motion. (f) Contrasting global and local deformations that occur in hybrid patterns leading to mode-locking behavior. In (e), (f), the green lines represent the panel diagonals, whose projections provides a clean way of sketching the motions.

pattern, the switching of Poisson's ratio can be tuned to occur at different fold angles by smoothly modifying the number of Miura mode strips in the system (see Section VII-B of the Supplementary Material), which renders the Morph pattern reprogrammable.

The hybrid patterns also exhibit interesting behavior in bending due to the combined action from Miura and Eggbox mode cells (see Movie 3 of the Supplementary Material). For example, a hybrid pattern with alternating Miura and Eggbox mode strips bends into a dome shape (Fig. 4(a)) whereas that with a set a of Miura mode strips adjacent to one another bends into a complex geometry that has both saddle and dome shapes (Fig. 4(b)).

The interplay between the contrasting Poisson's ratios of the Eggbox and Miura mode unit cells coupled with the global Poisson's ratio of the hybrid pattern leads to *mode-locking* behavior. The most obvious mode-locking is the tensile mode-locking (demonstrated in Movie 1 of the Supplementary Material). For certain types of hybrid modes, if we stretch the hybrid pattern along the **L** (axial) direction, the Miura mode cells, which normally would smoothly transition into Eggbox mode under stretching, would rather lock themselves in Miura mode and fold toward flat-folded state II. Tensile mode-locking happens when a hybrid pattern displays a positive Poisson's ratio globally, such that it shrinks in the lateral direction under stretching. For a Miura mode unit cell, this means that it must contract in the axial direction (as well as the lateral direction), despite that the global pattern is expanding in the axial direction in which it is stretched, as illustrated in Fig. 4(f). Similarly, compressive mode-locking happens to Eggbox unit cells when a hybrid pattern with globally negative Poisson's ratio is contracted (see Section VII-C of the Supplementary Material). We remark that the mode-locking of a hybrid Morph pattern is topological. It locks the mountain/valley assignment of certain unit cells, but still allows the pattern to fold smoothly as a rigid origami to the flat-folded states. This is different from motion locking [21] where the panels come into contact with each other hindering the rigid foldability and preventing the pattern from reaching the flat-folded state.

The Morph pattern exhibits morphing characteristics by breaking mountain/valley assignment, which leads to smooth switching of Poisson's ratio across a very wide range of negative to positive values, and topological mode-locking as a consequence of kinematic bifurcation. Our analysis reveals that the Morph pattern exhibits Poisson's ratio with equal magnitude but opposite sign when subject to in-plane and out-of plane deformations. Moreover, we discuss hybrid patterns that can be created by coupling Morph unit cells in distinct modes, creating a tessellation with reprogrammable Poisson's ratio and topological mode-locking. The locking feature of the hybrid patterns can be useful in creating structures with multi-stability [3]. We envision that hybrid patterns can also have many applications in topological mechanics due their ability to transform the symmetry of the system under in-plane deformations [22, 23].

We acknowledge useful discussions with Prof. David Zeb Rocklin. We thank the support from the US National Science Foundation (NSF) through grant no.1538830, the China Scholarship Council (CSC), and the Raymond Allen Jones Chair at Georgia Tech.

* P.P.P. and K.L. contributed equally to this work.
† Corresponding author: paulino@gatech.edu

[1] J. T. Overvelde, J. C. Weaver, C. Hoberman, and K. Bertoldi, Nature **541**, 347 (2017).
[2] E. T. Filipov, T. Tachi, and G. H. Paulino, Proceedings of the National Academy of Sciences **112**, 12321 (2015).
[3] S. Waitukaitis, R. Menaut, B. G.-g. Chen, and M. van Hecke, Physical Review Letters **114**, 055503 (2015).
[4] E. Boatti, N. Vasios, and K. Bertoldi, Advanced Materials **29** (2017).
[5] S. Li, H. Fang, and K. Wang, Physical Review Letters **117**, 114301 (2016).
[6] J. L. Silverberg, A. A. Evans, L. McLeod, R. C. Hayward, T. Hull, C. D. Santangelo, and I. Cohen, Science **345**, 647 (2014).
[7] L. H. Dudte, E. Vouga, T. Tachi, and L. Mahadevan, Nature Materials **15**, 583 (2016).
[8] M. Schenk and S. D. Guest, Proceedings of the National Academy of Sciences **110**, 3276 (2013).
[9] Z. Y. Wei, Z. V. Guo, L. Dudte, H. Y. Liang, and L. Mahadevan, Physical Review Letters **110**, 215501 (2013).
[10] C. Lv, D. Krishnaraju, G. Konjevod, H. Yu, and H. Jiang, Scientific Reports **4** (2014).
[11] M. Eidini and G. H. Paulino, Science Advances **1**, e1500224 (2015).
[12] H. Nassar, A. Lebée, and L. Monasse, Proceedings of the Royal Society - A **473**, 20160705 (2017).
[13] M. Schenk, *Folded shell structures*, Ph.D. thesis, University of Cambridge (2012).
[14] D. T. Ho, S.-D. Park, S.-Y. Kwon, K. Park, and S. Y. Kim, Nature Communications **5**, 3255 (2014).
[15] H. Yasuda and J. Yang, Physical Review Letters **114**, 185502 (2015).
[16] A. Rafsanjani and D. Pasini, Extreme Mechanics Letters **9**, 291 (2016).
[17] A. Rafsanjani and K. Bertoldi, Physical Review Letters **118**, 084301 (2017).
[18] J. Liu and Y. Zhang, Soft Matter **14**, 693 (2018).
[19] E. T. Filipov, K. Liu, T. Tachi, M. Schenk, and G. H. Paulino, International Journal of Solids and Structures **124**, 26 (2017).
[20] R. M. Murray, Z. Li, and S. S. Sastry, *A mathematical introduction to robotic manipulation* (CRC press, 1994).
[21] H. Fang, S. Li, and K. W. Wang, Proceedings of the Royal Society - A **472**, 20160682 (2016).
[22] B. G.-g. Chen, B. Liu, A. A. Evans, J. Paulose, I. Cohen, V. Vitelli, and C. Santangelo, Physical Review Letters **116**, 135501 (2016).
[23] D. Z. Rocklin, S. Zhou, K. Sun, and X. Mao, Nature Communications **8**, 14201 (2017).